Early doors (*Edo*) mutant mouse reveals the importance of period 2 (PER2) PAS domain structure for circadian pacemaking

Stefania Militi[a,1], Elizabeth S. Maywood[b,1], Colby R. Sandate[c], Johanna E. Chesham[b], Alun R. Barnard[a,2], Michael J. Parsons[a], Jennifer L. Vibert[a], Greg M. Joynson[a], Carrie L. Partch[c], Michael H. Hastings[b], and Patrick M. Nolan[a,3]

[a]Medical Research Council Harwell, Harwell Science and Innovation Campus, Oxfordshire OX11 0RD, United Kingdom; [b]Division of Neurobiology, Medical Research Council Laboratory of Molecular Biology, Cambridge Biomedical Campus, Cambridge CB2 0QH, United Kingdom; and [c]Department of Chemistry and Biochemistry, University of California, Santa Cruz, CA 95064

Edited by Joseph S. Takahashi, Howard Hughes Medical Institute, University of Texas Southwestern Medical Center, Dallas, TX, and approved January 26, 2016 (received for review September 2, 2015)

The suprachiasmatic nucleus (SCN) defines 24 h of time via a transcriptional/posttranslational feedback loop in which transactivation of *Per* (period) and *Cry* (cryptochrome) genes by BMAL1–CLOCK complexes is suppressed by PER–CRY complexes. The molecular/structural basis of how circadian protein complexes function is poorly understood. We describe a novel *N*-ethyl-*N*-nitrosourea (ENU)-induced mutation, early doors (*Edo*), in the PER-ARNT-SIM (PAS) domain dimerization region of period 2 (PER2) (I324N) that accelerates the circadian clock of $Per2^{Edo/Edo}$ mice by 1.5 h. Structural and biophysical analyses revealed that *Edo* alters the packing of the highly conserved interdomain linker of the PER2 PAS core such that, although $PER2^{Edo}$ complexes with clock proteins, its vulnerability to degradation mediated by casein kinase 1ε (CSNK1E) is increased. The functional relevance of this mutation is revealed by the ultrashort (<19 h) but robust circadian rhythms in $Per2^{Edo/Edo}$; $Csnk1e^{Tau/Tau}$ mice and the SCN. These periods are unprecedented in mice. Thus, $Per2^{Edo}$ reveals a direct causal link between the molecular structure of the PER2 PAS core and the pace of SCN circadian timekeeping.

mouse mutant | behavior | protein stability | circadian period | genetic interaction

Circadian rhythms, as exemplified by the sleep/wake cycle, are the outward manifestation of a 24-h timing mechanism that coordinates many physiological processes (1). The principal circadian clock in mammals is the suprachiasmatic nucleus (SCN). At a molecular level, the SCN clockwork consists of interacting positive and negative transcriptional/translational feedback loops (TTFLs) that drive rhythms in the RNA and protein levels of key clock components. Heterodimers of the PER-ARNT-SIM (PAS) domain-containing transcriptional activators CLOCK and BMAL1 drive rhythmic transcription of *Per* (period) and *Cry* (cryptochrome) genes by binding to E-box elements. PER proteins associate with CRY, translocating to the nucleus to inhibit their own transcription by interacting with the CLOCK–BMAL1 complex (2, 3). An additional feedback loop involves the nuclear orphan receptors REV-ERBα (4) and RAR-related orphan receptor A (RORA) (5) that modify the transcription of *Bmal1*, thereby stabilizing and amplifying the CLOCK–BMAL complex-dependent oscillation. Once suppressed, CLOCK–BMAL complex-mediated transactivation can only reoccur after PER and CRY have been degraded.

The circadian TTFL is therefore sustained by timely synthesis and degradation of PER and CRY proteins. Changes in PER stability in flies (6, 7) and changes in PER or CRY stability in mammals lead to a faster or slower clock (8). Phosphorylation-dependent licensing of PER proteins for ubiquitination and subsequent proteasomal degradation is a sensitive checkpoint in setting clock speed (9–11). Moreover, two familial advanced sleep phase syndromes (FASPSs) are associated with site-specific phosphorylation of human period 2 (PER2) (12, 13). Finally, the *Tau* mutation of casein kinase 1ε (*Csnk1e*) (14) is a hypermorph that accelerates the clock of rodents (15). Thus, phosphorylation, PER protein stability, and circadian period are intimately linked (16).

Current knowledge of the structural basis of circadian transcription and its repression is limited, but it is becoming clear that modular PAS domains form protein interactions that are important for progression of the circadian TTFL. The crystal structures of mouse CLOCK and BMAL1 have revealed how tandem PAS domains contribute to the formation of the dimeric transcription factor (17). PAS domains are also found in circadian negative regulators: tandem PAS domains mediate formation of PER dimers observed in vivo (18). Unlike the asymmetrical, extended conformation seen in CLOCK-BMAL1, the PER PAS dimer core forms a more symmetrical and compact fold (19, 20). In PER2, the PAS domain core is followed immediately by a CK1ε-dependent phosphodegron that recruits the E3 ubiquitin ligase β-TrCP to control PER2 stability (10, 16, 21). Thus, control of PER2 repressive function and/or PER2 stability may be controlled by interactions of its PAS domain core.

Significance

In a study investigating mechanisms whereby period 2 (PER2) stability can set the pace of biological rhythms, we have looked at molecular, cellular, and structural features of the mouse mutant, early doors (*Edo*). Early doors is a novel *N*-ethyl-*N*-nitrosourea (ENU)-induced point mutation that shortens the circadian period of mice by 1.5 h. The mutation results in an amino acid substitution in the interdomain linker between the tandem PAS domains of PER2. Biophysical analyses confirm that increased flexibility of this interdomain linker reduces stability of the PAS domain core. This flexibility can accelerate circadian rhythms by destabilizing the $PER2^{Edo}$ protein through faster kinase-mediated degradation. Furthermore, we find that $Per2^{Edo}$ mice carrying the casein kinase 1ε (*Csnk1e*) *Tau* mutation have extremely fast but very stable circadian clocks.

Author contributions: C.L.P., M.H.H., and P.M.N. designed research; S.M., E.S.M., C.R.S., J.E.C., A.R.B., M.J.P., G.M.J., C.L.P., and M.H.H. performed research; J.L.V. contributed new reagents/analytic tools; E.S.M., M.J.P., J.L.V., C.L.P., M.H.H., and P.M.N. analyzed data; and E.S.M., C.L.P., M.H.H., and P.M.N. wrote the paper.

The authors declare no conflict of interest.

This article is a PNAS Direct Submission.

Freely available online through the PNAS open access option.

Data deposition: Scattering datasets, analysis, and models have been deposited with BioISIS (www.bioisis.net) [deposition codes PLCSWP ($PER2^{WT}$) and PLCSEP ($PER2^{Edo}$)].

[1]S.M. and E.S.M. contributed equally to this work.

[2]Present address: Nuffield Department of Clinical Neurosciences, University of Oxford, Oxford OX3 9DU, United Kingdom.

[3]To whom correspondence should be addressed. Email: p.nolan@har.mrc.ac.uk.

This article contains supporting information online at www.pnas.org/lookup/suppl/doi:10.1073/pnas.1517549113/-/DCSupplemental.

To gain new insight into the mechanisms that determine the pace of the mammalian circadian clock, we used *N*-ethyl-*N*-nitrosourea (ENU) mutagenesis (22). We identified a founder mouse with a significantly shortened circadian period. The mutation, early doors (*Edo*), mapped to the *Per2* gene within the linker between the PAS-A and PAS-B domains. $PER2^{Edo}$ reveals the determinative relationship between protein stability and circadian pacemaking, and, more importantly, it reveals a structural framework within which to understand this defining property of the circadian system.

Results

***$Per2^{Edo}$* Shortens Circadian Wheel-Running Period.** We screened for genetic factors affecting overt behavioral circadian rhythms by monitoring daily wheel-running activity in progeny of ENU mutagenized mice. Within G1/dominant inheritance screens, we identified a mouse with a significantly shortened circadian period (τDD) (Fig. 1*A*). Test mating confirmed semidominant heritability of the phenotype, with the following mean circadian periods recorded in outcross/intercross offspring: WT τDD of ∼23.6 h, heterozygote τDD of ∼23 h, and homozygote τDD of ∼22 h (Fig. 1 *B* and *C*). Homozygotes also displayed a clear advanced phase of entrainment, with activity onsets preceding the onset of the dark phase by several hours. This mutant line was named early doors (*Edo*; Mouse Genome Informatics accession ID MGI:3606316).

The mutation was mapped by genetic linkage analysis to a 76.5-Mb region of mouse chromosome 1 (Fig. 1*D*). Within this region lies the period homolog 2 (*Per2*). With an established role in the circadian oscillator, this gene was selected as a candidate, and the coding regions of *Per2* were resequenced in a mutant animal. Sequencing revealed a T-to-A transversion in exon 9 of the gene (Fig. 1*E*). This nonsynonymous missense mutation results in an Ile-to-Asn substitution at residue 324 (I324N) of PER2, which lies in the interdomain linker between two tandem PAS domains (Fig. 1*F*). The residue is highly conserved within the protein sequence of all mouse *Per* genes and in the orthologous genes of other vertebrates.

***$Per2^{Edo}$* Is a Gain-of-Function Allele.** Several null alleles of *mPer2* have been described, and have been shown to have either no effect on circadian period (23) or to disrupt rhythms (24, 25). To define the genetic status of the $Per2^{Edo}$ allele, we created compound heterozygous mice alongside single mutants and controls and then monitored wheel-running behavior. The *Per2* genotype had an overall significant effect on the period of behavioral rhythms (1× ANOVA $F = 22.4$; 3,20 df; $P < 0.001$; Fig. 2*A*). Whereas $Per2^{Edo/Edo}$ mice exhibited accelerated period compared with WT (period: $Per2^{+/+} = 23.9 \pm 0.1$ h, $Per2^{Edo/Edo} = 22.4 \pm 0.2$ h; $n = 3, 6$; $P < 0.01$), $Per2^{-/-}$ mice had periods (24.0 ± 0.2 h; $n = 6$) not significantly different from WT and significantly ($P < 0.01$) longer than $Per2^{Edo/Edo}$. Moreover, the period of $Per2^{Edo/-}$ compound heterozygotes (23.5 ± 0.1 h; $n = 9$) was intermediate between $Per2^{Edo/Edo}$ and $Per2^{-/-}$ mutants, although still significantly ($P < 0.01$) longer than the period of $Per2^{Edo/Edo}$. At a behavioral level, therefore, $Per2^{Edo}$ is not a loss-of-function mutation. To explore the dose dependence of this effect, SCN slices were prepared from *Per1-Luc* reporter mice, heterozygous or homozygous for $Per2^{Edo}$. As with behavior, heterozygous mice showed a period acceleration of 0.56 h, and a second copy of $Per2^{Edo}$ accelerated the clock further, to 1.23 h shorter than WT (1× ANOVA $F = 5.0$; 2,36 df; $P < 0.02$; $Per2^{+/+}$ vs. $Per2^{Edo/Edo}$: $t = 3.1$, $P < 0.05$; Fig. 2*B*). There was no effect of $Per2^{Edo}$ genotype on the amplitude of oscillation reported by *Per1-luc*. We then examined SCN function in compound heterozygotes and controls using the *Per1-luc* reporter (Fig. 2*C*). As with behavioral rhythms, *Per2* genotype had an overall effect on circadian period (1× ANOVA $F = 39.4$; 2,55 df; $P < 0.001$). The SCN of $Per2^{-/-}$ mice had a period comparable to WT SCN (period: $Per2^{+/+} = 23.9 \pm 0.1$ h, $Per2^{-/-} = 23.8 \pm 0.1$ h; $n = 9$). In contrast, but consistent with behavioral findings, $Per2^{Edo}$ dose-dependently accelerated the SCN clock. The period of SCN from $Per2^{Edo/Edo}$ mice was significantly shorter than the period of SCN from $Per2^{-/-}$ mice, and in compound heterozygous $Per2^{Edo/-}$ mice, the single copy of $Per2^{Edo}$ shortened the period to a value not different from the period

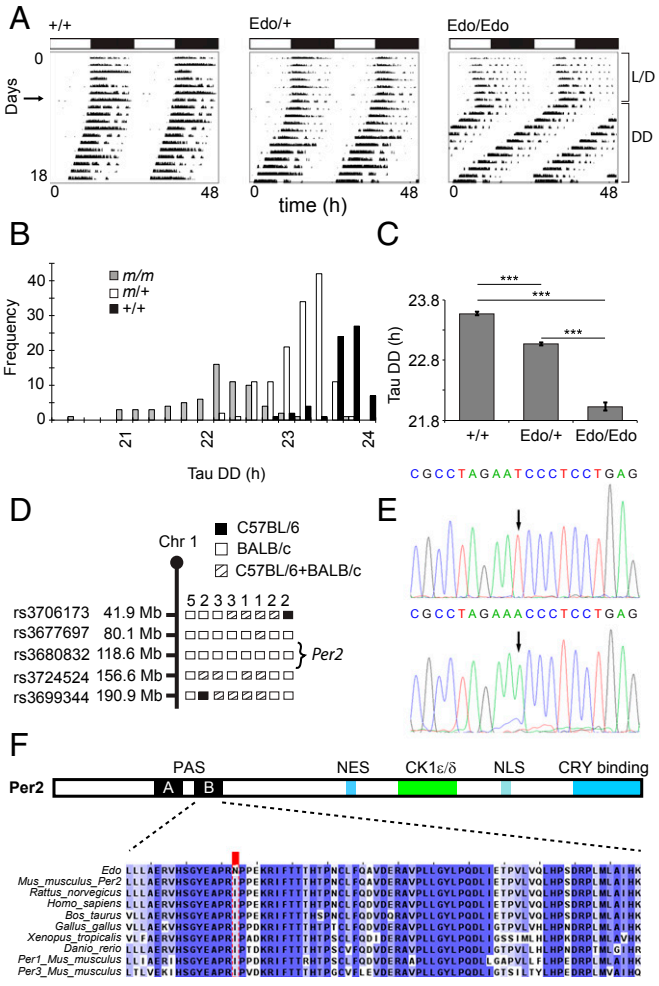

Fig. 1. Phenotype and cloning of the $Per2^{Edo}$ mutation. (*A*) Representative double-plotted actograms of wheel-running activity of +/+, *Edo*/+, and *Edo/Edo* mice, recorded under light/dark (L/D) conditions (days 1–7) followed by constant darkness (DD). Horizontal bars at the top indicate L/D conditions over the first 7 d. (*B*) Frequency distribution of the endogenous period [Tau DD (τ_{DD})] of WT (+/+, black), *Edo*/+ (*m*/+, white), and *Edo/Edo* (*m/m*, gray) littermates. (*C*) Free-running period of mutants and littermate controls in constant darkness (mean ± SEM; $n = 66, 134, 70$; one-way ANOVA, $P < 0.001$; ***Bonferroni pairwise comparisons, $P < 0.001$). (*D*) Graphical representation of chromosome 1 (Chr 1) showing positions of SNP markers used to genotype the affected animals. Informative haplotypes for phenotypically homozygous animals are indicated. (*E*) Chromatograms from resequencing the *Per2* gene in +/+ (*Top*) and *Edo/Edo* (*Bottom*) DNA. (*F*) Functional domains of PER2 (*Top*) and sequence conservation in PER2 (*Bottom*) proteins. CK1ε/δ, CK1ε/δ binding domain; NES, nuclear export signal; NLS, nuclear localization signal. The protein sequence alignment of the interdomain linker and PAS-B domain showing the I324N substitution (red box) in $Per2^{Edo}$ is illustrated. High sequence conservation of the interdomain linker and PAS-B domain is evident in vertebrate proteins and in paralogous mouse proteins (PER1, PER3).

seen in $Per2^{Edo/+}$ SCN but shorter than in $Per2^{-/-}$ SCN (1× ANOVA $F = 39.4$; 2,55 df; $P < 0.001$; $Per2^{-/-}$ vs. $Per2^{Edo/-}$: $t = 1.8$ ns; $Per2^{-/-}$ vs. $Per2^{Edo/Edo}$: $t = 7.2$, $P < 0.001$; $Per2^{Edo/-}$ vs. $Per2^{Edo/Edo}$: $t = 7.5$, $P < 0.001$). Thus, data from SCN ex vivo studies support the behavioral observations that $Per2^{Edo}$ is a gain-of-function, probably antimorphic, mutation.

We tested whether the accelerated $Per2^{Edo}$ SCN affected peripheral clocks. The liver of $Per2^{Edo/Edo}$ mice held on a 24-h light/dark (L/D) schedule exhibited very robust daily cycles of gene expression, with amplitudes comparable to the amplitudes of liver from WT mice (Fig. S1). There was a marked advance of *ca.* 3 h in the phase of the peripheral oscillations for both core clock genes

NEUROSCIENCE

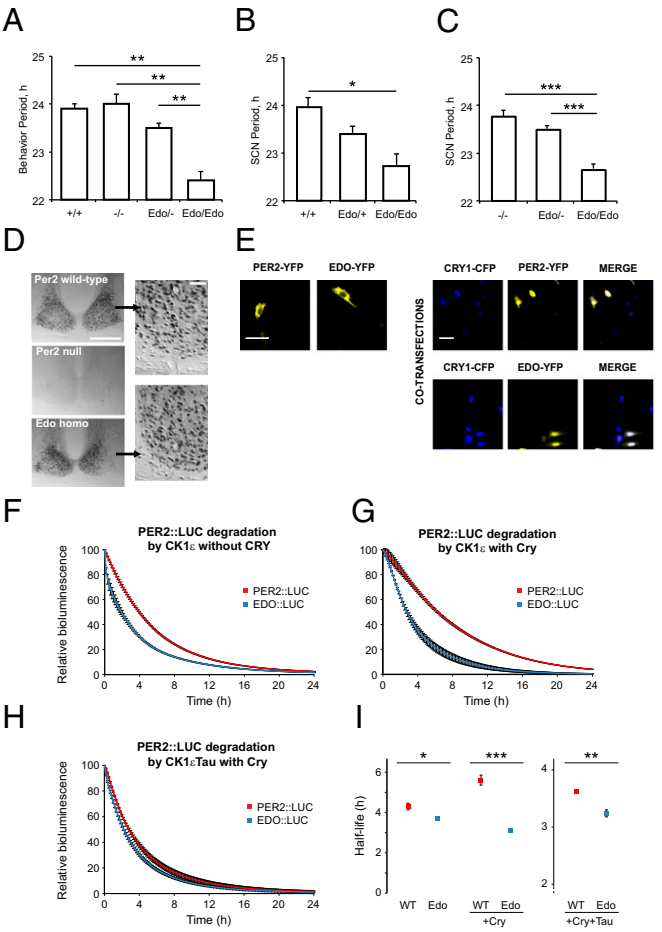

Fig. 2. Reporter oscillations and PER2 stability are affected in $Per2^{Edo}$. (*A*) Comparison of wheel-running period in $Per2^{-/-}$, $Per2^{Edo/Edo}$, and $Per2^{Edo/-}$ compound heterozygous mutants with littermate controls in constant darkness. (*B*) Circadian period reported by *Per1-luc* bioluminescence of SCN slices from WT, $Per2^{Edo/+}$, and $Per2^{Edo/Edo}$ mice. (*C*) Circadian period reported by *Per1-luc* bioluminescence of SCN slices from $Per2^{-/-}$, $Per2^{Edo/-}$, and $Per2^{Edo/Edo}$ mice. (*D*) Immunostaining of PER2 in SCN of WT, $Per2^{-/-}$ (null), and $Per2^{Edo/Edo}$ mice at Zeitgeber time 12. (Scale bar, 500 μm.) (*Insets*) Nuclear localization of PER2. (Scale bar, 50 μm.) (*E*) Nuclear/cytoplasmic distribution of YFP-tagged $PER2^{WT}$ and $PER2^{Edo}$ in COS7 cells, transfected alone or with CFP-CRY1. A representative experiment of three independent experiments is shown. (Scale bars, 100 μm.) (*F–H*) Graphs showing decay of PER2::LUC and EDO::LUC bioluminescence in cycloheximide-treated HEK293 cells. Conditions are as indicated on each graph ($n = 3$ per condition, mean ± SEM). (*I*) Comparison of $t_{1/2}$ of bioluminescent decay for each condition depicted in *F–H* (*$P < 0.05$; **$P < 0.01$; ***$P < 0.001$ by *t* test).

(*Bmal1*, *Per1*, *Per2*, and *Cry1*) and the canonical circadian output gene *Dbp*. This phase advance is likely a consequence of the advanced phase of the behavioral rhythm exhibited in the homozygous mutants when entrained to the L/D cycle (Fig. 1*A*). Thus, the shortened period of the $Per2^{Edo/Edo}$ SCN, and perhaps also an accompanying acceleration of the local liver clock, had a significant effect on peripheral circadian organization.

Finally, to confirm that $Per2^{Edo}$ is not a null allele, serial sections of SCN were immunostained with anti-PER2 serum (26). In WT SCN collected at the peak of PER2 expression (Zeitgeber time 12, lights-off), nuclear immunolabeling was extensive across the SCN (Fig. 2*D*). In homozygous PER2-null SCN, immunolabeling was absent. In contrast, SCN from $Per2^{Edo/Edo}$ mice exhibited widespread nuclear immunoreactivity, comparable to the nuclear immunoreactivity of WT (cell counts: $Per2^{+/+} = 413 \pm 26$; $Per2^{Edo/Edo} = 256 \pm 53$; $Per2^{-/-} = 2 \pm 1$; $n = 3$ per group; 1× ANOVA $F = 36.3$; 2,6 df; $P < 0.001$; $Per2^{+/+}$ vs. $Per2^{Edo/Edo}$: t = 3.2 ns; $Per2^{+/+}$ vs. $Per2^{-/-}$: t = 8.4, $P < 0.001$; $Per2^{Edo/Edo}$ vs. $Per2^{-/-}$: t = 5.2, $P < 0.01$). $Per2^{Edo}$ thus encodes a PER2 variant highly expressed and trafficked appropriately to the nucleus of SCN neurons.

$PER2^{Edo}$ Maintains Its Ability to Dimerize but Is Less Stable than $PER2^{WT}$. To characterize the biochemical properties of $PER2^{Edo}$ likely to underpin the accelerated clock, we initially focused on protein dimerization, a function determined by the PAS domains where the mutation is located. PER2 PAS domains mediate the formation of homodimers and heterodimers with both PER1 and PER3 (19, 20). Using site-directed mutagenesis, we created the I324N mutation in full-length PER2 and expressed proteins in COS7 cells with various C-terminal tags. Immunoblotting of cell lysates confirmed the appropriate expression of all tagged proteins (Fig. S2 *A–C*). Coimmunoprecipitation showed that $PER2^{Edo}$ exhibited the expected homodimerization and associations with CRY2, whereas minimal interactions were found with REV-ERBα and BMAL1. Importantly, $PER2^{Edo}$ exhibited comparable associations that, within the limits of the assay, were not significantly different from the associations of $PER2^{WT}$ (Fig. S2*D*). Given that association with CRY is thought to direct nuclear translocation of PER, we expressed tagged PER2 and CRY1 and monitored their cellular localization. In the absence of CRY1, both PER2 variants were predominantly cytoplasmic (Fig. 2*E*). Cotransfection with CRY1, however, localized both variants to the nucleus. Thus, the mutation did not compromise functional interaction between PER2 and CRY1, and it did not appear to affect the subcellular localization of either.

Steady-state analyses of the intracellular behavior of $PER2^{Edo}$ failed to reveal significant effects of the mutation. Given that nuclear localization and complex formation can influence the degradation of circadian proteins, we monitored the real-time decay of bioluminescent PER2::LUC fusion proteins in HEK293 cells to test the relative vulnerability of $PER2^{Edo}$ to proteasomal degradation triggered by CK1ε (15). Following treatment with the translational inhibitor cycloheximide, bioluminescent signal for cytoplasmic PER2::LUC declined progressively in the presence of CK1ε. Degradation of EDO::LUC, however, was more rapid (Fig. 2 *F* and *I*). The $t_{1/2}$ of EDO::LUC was slightly but significantly shorter (36 min) than PER2::LUC ($P = 0.0223$, *t* test). In the presence of CRY, the vulnerability of nuclear EDO::LUC to CK1ε-mediated degradation was even more pronounced (151 min shorter; $P = 0.0005$, *t* test; Fig. 2 *G* and *I*). Although the $t_{1/2}$ of nuclear PER2::LUC was substantially longer in this study, the EDO::LUC $t_{1/2}$ was shorter. Finally, coexpression with $CK1\varepsilon^{Tau}$ in the presence of CRY resulted in a consistent shorter $t_{1/2}$ in EDO::LUC (23 min; $P = 0.0035$, *t* test; Fig. 2 *H* and *I*). Thus, although the Edo mutation did not prevent $PER2^{Edo}$ from forming complexes with other circadian proteins, the vulnerability of $PER2^{Edo}$ to CK1ε-mediated degradation was nevertheless greater.

$PER2^{Edo}$ Increases Flexibility of Interdomain Linker to Destabilize the PAS Domain Core of PER2. The *Edo* mutation is located in a conserved linker between the two PAS domains that is distant from the dimer interface observed in the crystal structure (19), consistent with our finding that *Edo* does not have an impact on dimerization in full-length proteins or in the purified tandem PAS domains [PAS-A and PAS-B (PAS-AB) domains; Fig. S3 *A* and *B*]. However, we reasoned that substitution of the more polar Asn at this site might disrupt packing of the linker to influence conformation of the $PER2^{Edo}$ PAS-AB dimer in solution. This possibility was assessed using small-angle X-ray scattering (SAXS), which provides low-resolution envelopes of protein structures in solution (27). Scattering curves for $PER2^{WT}$ and $PER2^{Edo}$ were essentially identical and confirmed dimer formation (Fig. S3 *C–E*). The pair-distance distribution function (Fig. 3*A*) indicated that both PAS-AB dimers maintain a compact fold in solution, as demonstrated by oblate spherical envelopes that were well fit by the PAS-AB structure with missing loops modeled in Fig. 3*B* and Fig. S3 *F* and *G*. We then used differential scanning fluorimetry to assess thermodynamic stability of the two proteins. We found that the $PER2^{Edo}$ PAS dimer core was significantly less stable than $PER2^{WT}$,

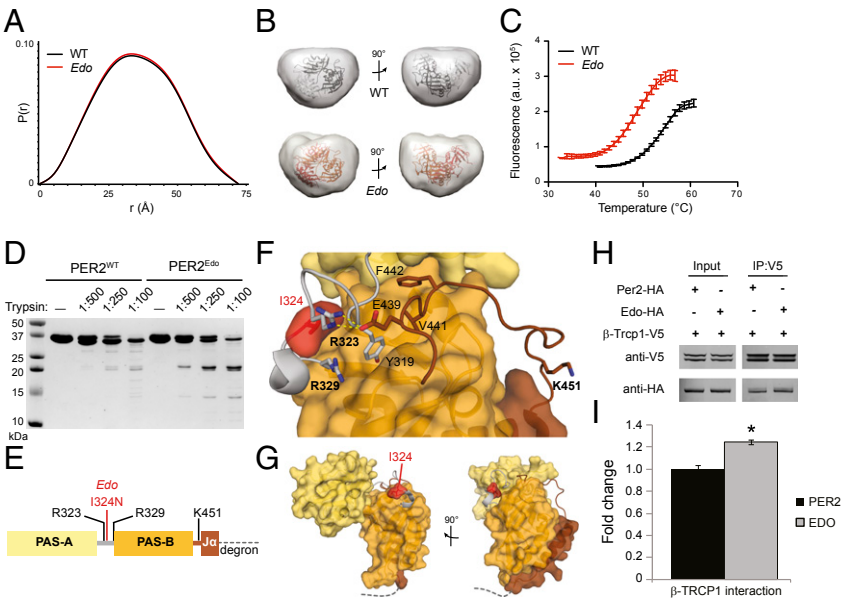

Fig. 3. PER2^{Edo} mutation increases flexibility of the interdomain linker to destabilize the PAS domain core. (*A*) SAXS pairwise distribution curves for the PAS-AB dimer of PER2^{WT} (black) or PER2^{Edo} (red). (*B*) Envelopes calculated from SAXS data for PER2^{WT} and PER2^{Edo} PAS-AB dimers fitted with the crystal structure (Protein Data Bank ID code 3GDI). (*C*) Thermal denaturation curves of purified proteins in the presence of SYPRO Orange dye (Sigma–Aldrich). Mean fluorescence ($n = 6$ from one representative experiment) is shown with SD error bars. T_ms derived from nonlinear regression: PER2^{WT}, 54.6 ± 0.4 °C; PER2^{Edo}, 49.4 ± 0.3 °C. a.u., arbitrary units. (*D*) Limited proteolysis of His_6-tagged proteins with indicated ratios of trypsin (wt/wt) for 1 h at room temperature. Cleavage products were resolved by 18% SDS/PAGE and visualized by Coomassie staining. (*E*) Schematic of the PER2 PAS-AB domain region with trypsin cleavage sites determined by liquid chromatography/MS. The dashed line represents the phosphodegron immediately downstream of the Jα helix. (*F*) Close-up view of the interdomain and Jα helix linkers in the PER2 PAS-AB domain core. Domain coloring is as in *E*; trypsin cleavage sites detected by liquid chromatography/MS are shown in bold. (*G*) Relationship of PAS domains, *Edo* and Jα helix to the PER2 phosphodegron (dashed line). (*H*) Representative Western blots of lysates (Input) from HEK293 cells transfected with either WT (Per2) or mutant (Edo) PER2-HA and V5-tagged TRCP1 immunoprecipitated (IP) with an Ab to V5. (*I*) Relative differences in protein interactions were determined by normalizing the amount of coimmunoprecipitated proteins to the amount of the primary precipitated protein. Values represent the mean ± SEM of four independent experiments (*$P < 0.05$, *t* test).

exhibiting a decrease in melting temperature (T_m) of more than 5 °C (Fig. 3*C*), which corresponds to a change in the free energy of unfolding, ΔΔG, of 0.66 kcal/mol at the WT T_m of 54.6 °C. Therefore, *Edo* decreases the intrinsic stability of the PER2 PAS domain core without causing global changes in the overall structure.

To determine how *Edo* influences stability of the PAS domain core, we probed flexibility of the protein backbone using limited proteolysis. Digestion with chymotrypsin showed no difference between PER2^{WT} and PER2^{Edo} (Fig. S3*H*), but we observed a pattern of differential cleavage by trypsin (Fig. 3*D*): first, a short peptide was preferentially cleaved from the C terminus of PER2^{WT}; second, PER2^{Edo} preferentially accumulates ∼21-kDa fragments (Fig. S3 *I* and *J*). Specific cleavage sites were identified by liquid chromatography/MS. Cleavage at K451 in the linker to the Jα helix occurred preferentially in PER2^{WT}, whereas cleavage of the interdomain linker at R323 and R329 occurred preferentially in PER2^{Edo} (Fig. 3*E*). The interdomain and Jα linkers interact with one another and the PAS-B domain through hydrophobic packing and electrostatic interactions, including a salt bridge between R323 and E439 (Fig. 3*F*). This network of interactions suggests how *Edo* could influence the flexibility of two linkers that are separated by the PAS-B domain in the primary sequence (Fig. S3*K*).

The phosphodegron that regulates CK1ε-dependent turnover of PER2 is located immediately downstream of the Jα helix (Fig. 3 *E* and *G*). The structure ends at P473 and is followed by the sequence HSGSSGYGS (residues 474–482), where phosphorylation by CK1ε at the underlined Ser residues facilitates binding of the E3 ubiquitin ligase β-TRCP1 (10, 16, 21). Therefore, alterations to the stability and flexibility of the PAS-AB domains may further contribute to destabilization of the mutant in vivo by altering accessibility of this motif. In support of this argument, we found a stronger interaction between β-TRCP1 and PER2^{Edo} when coimmunoprecipitated from HEK293 cell protein complexes ($P = 0.022$, *t* test; Fig. 3 *H* and *I*).

PER2^{Edo} Is More Sensitive to CK1ε-Mediated Degradation in Vivo, Generating an Extremely Rapid Circadian Clock. To test predictions based on our biochemical and biophysical analyses in vivo, we crossed the *Per2^{Edo}* mutation with the *Csnk1e^{Tau}* mutation. Our prediction was that availability of the more vulnerable PER2^{Edo} substrate would allow the mutant CK1ε to accelerate the circadian TTFL even further than in a *Per2$^{+/+}$* background. As anticipated, *Csnk1e$^{Tau/Tau}$* mice were unable to entrain to the 24-h lighting cycle regardless of whether they carried the additional *Per2$^{Edo/Edo}$* allele (Fig. 4 *A* and *B*), whereas mice carrying *Per2$^{Edo/Edo}$* alone could still entrain. Under continuous dim red light, the free-running periods revealed an additive effect of the two mutations. Both alleles contributed to a shortening of the behavioral circadian period, as revealed by significant main effects of *Csnk1e^{Tau}* and *Per2^{Edo}* by two-way ANOVA ($P < 0.0001$ for both). There was not, however, any interaction ($P = 0.35$). For each of the three *Csnk1e^{Tau}* genotypes tested, the periods of *Per2$^{Edo/Edo}$* mice were significantly shorter than the periods of *Per2$^{+/+}$* controls. Notably, the period of the double-homozygous animals was 18.80 ± 0.04 h, which is an unprecedentedly fast behavioral rhythm in mice, and comparable to the ultrashort period of "super-duper" hamsters (28).

To confirm that these additive genotypic effects occurred within the SCN, slices were made and the circadian period was determined by recording *Per1-luc* bioluminescence (Fig. 4*C*). As with behavior, both alleles contributed to a shortening of the circadian period (main effects two-way ANOVA: $P < 0.0001$ for both). Again, there was no interaction ($P = 0.18$), confirming their additive, independent actions. Thus, for all three *Csnk1e^{Tau}* genotypes tested, the periods of *Per2$^{Edo/Edo}$* SCN were significantly shorter than the periods of *Per2$^{+/+}$* controls, creating, again, an unprecedentedly short, genetically specified circadian period for the SCN of 18.80 ± 0.06 h.

Discussion

Edo is a novel ENU-induced mutation that shortens the circadian wheel-running period in mice, an effect mediated by accelerated molecular pacemaking in the SCN. The point mutation in *Edo* lies in the interdomain linker (I324N) between two PAS domains in PER2, and has the effect of increasing linker mobility and reducing stability of the core PAS dimer in PER2^{Edo} in vitro. This mutation is associated with increased vulnerability of PER2^{Edo} to CK1ε-dependent degradation in vivo. Thus, in *Per2^{Edo}*; *Csnk1e^{Tau}* mice, the combination of increased vulnerability of the substrate with the gain-of-function enzyme leads to extremely short circadian periods of behavior and SCN gene expression.

By uncovering a new allelic variant of *Per2*, the current study illustrates the continuing value of forward genetic screens to

NEUROSCIENCE

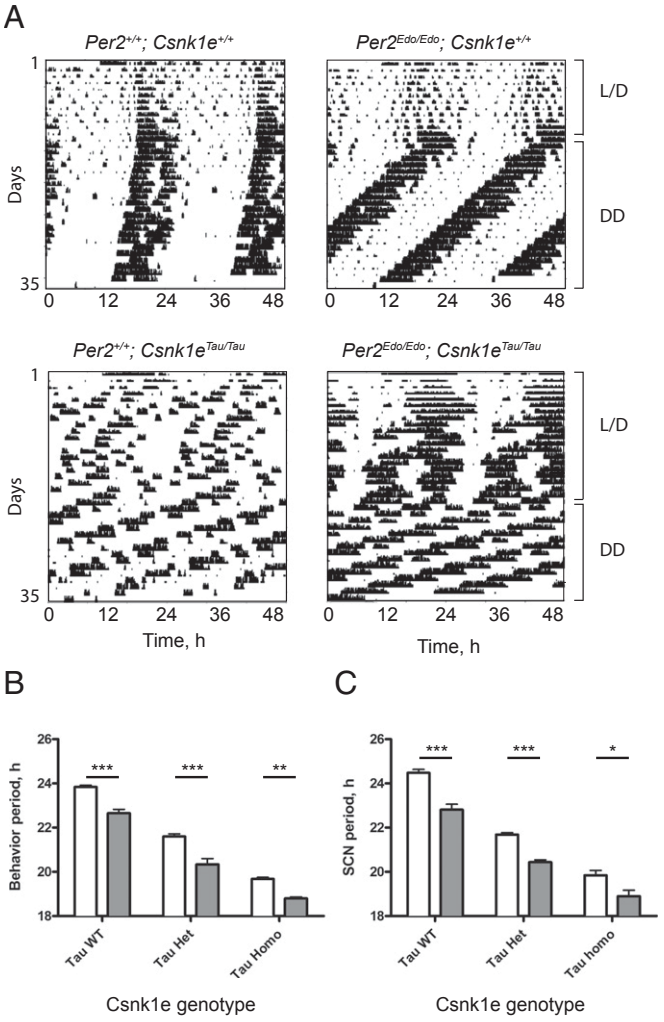

Fig. 4. *Per2$^{Edo/Edo}$; Csnk1e$^{Tau/Tau}$* double mutants have an extremely short circadian period in vivo and in vitro. (*A*) Representative double-plotted actograms of wheel-running for *Per2$^{+/+}$; Csnk1e$^{+/+}$*, *Per2$^{Edo/Edo}$; Csnk1e$^{+/+}$*, *Per2$^{+/+}$; Csnk1e$^{Tau/Tau}$*, and *Per2$^{Edo/Edo}$; Csnk1e$^{Tau/Tau}$* mice. Animals were entrained to cycles of 12-h L/D and then placed into continuous dim red light as indicated. (*B*) Circadian period of wheel-running activity rhythms from *Per2$^{+/+}$* (white bars) and *Per2$^{Edo/Edo}$* (gray bars) mice in the presence or absence of *Csnk1e^{Tau}* mutant alleles. (*C*) Circadian period reported by *Per1-luc* bioluminescence rhythms of SCN slices from *Per2$^{+/+}$* (white bars) and *Per2$^{Edo/Edo}$* (gray bars) mice in the presence or absence of *Csnk1e^{Tau}* mutant alleles (mean ± SEM; ***$P < 0.001$, **$P < 0.01$, *$P < 0.05$ by *t* test).

understand circadian mechanisms. The accelerated oscillation in the *Edo* SCN emphasizes the critical role of protein stability in setting the circadian period. The interaction between PER2 and CK1ε is clearly pace-setting, as revealed by accelerated clocks in mutants of CK1ε and CK1δ in rodents and humans, respectively, and in the human PER2 FASPS mutant (12) now alongside mouse PER2^{Edo}. These observations are consistent with the view that the rhythmic availability of PER2 "defines a critical nodal point for negative feedback" within the TTFL (29). Moreover, the *Edo* mutation accelerates/phase-advances mRNA rhythms in the liver that are, again, as well defined as the mRNA rhythms seen in WT animals. Thus, a genetic background that accelerates PER2 degradation generates an ultrashort <19-h circadian period in the SCN and in activity/rest cycles. In hamsters, a comparably fast period is seen in compound mutants for *Csnk1e^{Tau}* and "duper," an unidentified mutation that does not reside in hamster *Per2* (28). Critically, the rhythms in hamsters and mice alike are as robust and coherent as in the 24-h WT, highlighting the precision and stability of the SCN oscillator remaining unperturbed in the face of a >20% acceleration of the TTFL.

Importantly, *Edo* does not phenocopy the *Per2* null mutant. First, by immunostaining and circadian recording, it is clear that PER2^{Edo} is expressed and functional. Second, it displays semidominant inheritance, with progressively severe heterozygous and homozygous phenotypes. This phenotype is a notable variation from targeted deletions of *Per2*, which are phenotypically recessive. Third, this phenotype is expressed in the compound heterozygote *Per2$^{Edo/-}$*. It therefore acts as a gain-of-function mutation. We speculate that this gain of function is due to maintenance of normal interactions of PER2^{Edo} with other clock proteins (e.g., CRY), whereas its more rapid turnover leads to a change in the repressive "nodal set point" established by PER2 (29).

Having characterized the phenotypic consequences of the mutation in vivo, we explored its biochemical and structural features to discover that *Edo* destabilizes the PAS domain dimer core to accelerate PER2 degradation. Notably, *Edo* does not induce global changes in dimer structure as assessed by size-exclusion chromatography and SAXS. Here, we show that *Edo* alters the flexibility of linkers in the PAS domain core to elicit its dramatic overall effect on PER2 function. *Edo* makes the PAS domain core less intrinsically stable and also leads to increased interaction with its E3 ubiquitin ligase β-TRCP1, leading to increased turnover in vivo. Given the modest buried surface area between the interdomain linker and the PAS domains (590 Å^2), it is perhaps surprising that substitution of one residue has such profound implications for PER2 structure and function. However, the interdomain and Jα linkers are linked through a series of interactions on the PAS-B domain, potentially connecting the *Edo* site to the CK1ε-dependent phosphodegron immediately downstream of the Jα helix (16). The biochemical basis of the interaction between PER2 and CK1ε is, however, unclear. A current model posits that the Tau mutation changes the relative efficacy of CK1ε at two competing phosphorylation sites that determine whether PER2 has a fast or slow degradation rate (16). Further work will be necessary to understand the structural basis by which linker flexibility enhances interaction with CK1ε-dependent β-TRCP1 activity to control PER2 stability in vivo. Our data reaffirm the central role of PAS-mediated mechanisms in tuning the period of the mammalian circadian clock, and thereby extend the scope of molecular structure-based analysis of cellular timekeeping.

Methods

Animals. All animal studies were carried out in accordance with the 1986 Animals (Scientific Procedures) Act, United Kingdom, with Medical Research Council Harwell and Laboratory of Molecular Biology ethical approval and were compliant with the guidance issued by the Medical Research Council (30). Inbred strains were obtained from in-house stock (C57BL/6J, C3H/HeH; hereafter termed C3H) or were purchased from Harlan-Olac (BALB/cOlaHsd, hereafter termed BALB/c). Mutant and reporter lines were obtained from the following: D. Weaver [University of Massachusetts Medical School, Worcester, MA; Per2^{tm1Drw} null mutant (24)], H. Okamura [University of Kyoto, Kyoto; mPer1-luc reporter (31)], J. S. Takahashi [University of Texas Southwestern Medical Center, Dallas; mPer2::Luc reporter, Per2^{tm1Jt} (32)], and A. S. Loudon [University of Manchester, Manchester, United Kingdom; Ck1ε mutant, Csnk1e^{tm1Asil} (15)]. All molecular and behavioral studies were carried out in mice bred on a congenic C57BL/6J background.

Mutagenesis, Genetic Mapping, and Mutation Detection. Mutagenesis, screening, genetic linkage, positional candidate analysis, and sequencing were carried out as described previously (22, 33).

SCN Slices. SCN organotypic slices for bioluminescence recordings and immunostaining of SCN PER2 expression were as described previously (26).

Cell Culture and Transfection. COS7 and HEK293 cells were maintained in DMEM supplemented with 10% (vol/vol) FBS and antibiotics (100 μg/mL penicillin and streptomycin). Transient transfection was carried out using Fugene 6 (Roche) according to the manufacturer's protocol. For degradation studies, HEK293 cells were transfected with either PER2::LUC (a generous gift from Y.-H. Fu and A. Hirano, University of California, San Francisco, San

Francisco, CA) or EDO::LUC generated by site-directed mutagenesis (Stratagene). Reporter constructs were cotransfected with combinations of $CK1\varepsilon^{WT}$, $CK1\varepsilon^{Tau}$, and mCry2-HA plasmids. Bioluminescence degradation studies were conducted as in the study by Hirano et al. (34). Luciferase activity of PER-LUC was recorded at 10-min intervals at 37 °C with Lumicycle (Actimetrics). The data were fitted to an exponential curve of the form $N(t) = N_0\, e^{(-\lambda t)}$ where N(t) is the luminescence (counts per second) at time t, N_0 is the initial luminescence (counts per second), λ is the decay rate, and t is the time. The rate of λ was determined using a MATLAB (MathWorks) Curve Fitting Toolbox, and $t_{1/2}$ was calculated using the $t_{1/2}$ equation $t_{1/2} = \ln(2)/\lambda$.

For coimmunoprecipitation experiments, cells were transfected with $mPER2^{WT}$-V5-YFP-His, $mPER2^{Edo}$-V5-YFP-His, or β-TRCP1–V5-His plasmids and mCry2-HA, HA-mPER2, HA-$mPER2^{Edo}$, mBmal1-FLAG, mRev-erba-V5, respectively, in 10-cm dishes in medium without antibiotics. The total amount of transfected DNA was 6 μg (composed of 3 μg of mPer2 WT or mPer2 mutant and 3 μg of mCry2-HA, HA-mPer2, HA-mEdo, HA-mPer1, mBmal1-FLAG, mClock-HA, mRev-erba-V5). Forty-eight hours after transfection, cells were washed three times with cold PBS, lysed in 700 μL of lysis buffer, and treated as described above.

Coimmunoprecipitation and Western Blotting. Tagged proteins were immunoprecipitated from COS7 or HEK293 cell lysates with anti-V5 (R960-25; Invitrogen), anti-HA (HA.11; Covance), or anti-FLAG M2 (F3165; Sigma) following 2 h of gentle agitation at 4 °C with 25 μL of protein G agarose. Samples were washed in buffer, boiled at 95 °C for 5 min, separated by SDS/PAGE on a 4–12% gel, and transferred to a PVDF membrane. Immunoblotting was performed using anti-V5 (1:3,000), anti-HA (1:1,000), anti-FLAG (1:800), and anti-GFP (1:5,000) (11814460001; Roche). Secondary Ab was HRP-conjugated anti-mouse (Sigma) at a 1:10,000 dilution. Chemiluminescence was performed using ECL Plus (Amersham).

Recombinant Protein Expression and Purification. A fragment containing the tandem mouse PER2 PAS-AB domains (residues 170–473) was expressed in *Escherichia coli* as a fusion with a tobacco etch virus (TEV)-cleavable N-terminal His_6 tag. The *Edo* mutation (I324N) was introduced by site-directed mutagenesis and validated by sequencing. Protein expression was induced with 0.5 mM isopropyl β-D-1-thiogalactopyranoside at an OD_{600} of ∼0.8, and *E. coli* was grown for an additional 16 h at 18 °C. Soluble proteins were purified by Ni^{2+}-nitrilotriacetic acid affinity chromatography (QIAGEN), followed by cleavage of the His_6 tag with TEV protease for either 4 h at room temperature or overnight at 4 °C. Subsequent Ni^{2+}-nitrilotriacetic acid affinity chromatography was performed to remove the protease and cleaved tag. Proteins were further purified by size-exclusion chromatography on a Superdex 75 16/60 prep grade column (GE Healthcare) equilibrated in 25 mM Hepes (pH 7.5), 200 mM NaCl, and 5 mM DTT, and then concentrated to 10 mg/mL. Concentration of the purified, cleaved proteins (residues 170–473 with an N-terminal "GAMDP" remaining after TEV cleavage) was determined at A_{280} using a calculated extinction coefficient of 32,890 $M^{-1}{\cdot}cm^{-1}$.

ACKNOWLEDGMENTS. We thank Drs. Ying-Hui Fu and Arisa Hirano (University of California, San Francisco) for providing us with the PER2::LUC construct. We are grateful for excellent technical support from the Biomedical Staff at the Medical Research Council Mary Lyon Centre and the Ares facility. We thank Steve Thomas for work on the figures. SAXS data were collected at the Advanced Light Source (ALS), a national user facility supported by the US Department of Energy Office of Biological and Environmental Research. Additional support comes from the US NIH project MINOS R01 GM105404. We thank Greg Hura and Jane Tanamachi at the ALS SIBYLS beamline for their assistance. This study was supported by Medical Research Council, United Kingdom Grants MC_U142684173 and MC_U105170643; Sixth Framework Project EUCLOCK Grant 018741 (to M.H.H. and P.M.N.); and US NIH Grant R01 GM107029 (to C.L.P.). The University of California, Santa Cruz Mass Spectrometry Facility receives support from the W. M. Keck Foundation (Grant 001768) and the US NIH Center for Research Resources (Grant S10 RR020939).

1. Reppert SM, Weaver DR (2002) Coordination of circadian timing in mammals. *Nature* 418(6901):935–941.
2. Schibler U, Sassone-Corsi P (2002) A web of circadian pacemakers. *Cell* 111(7):919–922.
3. Koike N, et al. (2012) Transcriptional architecture and chromatin landscape of the core circadian clock in mammals. *Science* 338(6105):349–354.
4. Preitner N, et al. (2002) The orphan nuclear receptor REV-ERBalpha controls circadian transcription within the positive limb of the mammalian circadian oscillator. *Cell* 110(2):251–260.
5. Sato TK, et al. (2004) A functional genomics strategy reveals Rora as a component of the mammalian circadian clock. *Neuron* 43(4):527–537.
6. Shigeyoshi Y, et al. (2002) Restoration of circadian behavioural rhythms in a period null Drosophila mutant (per01) by mammalian period homologues mPer1 and mPer2. *Genes Cells* 7(2):163–171.
7. Yang Z, Sehgal A (2001) Role of molecular oscillations in generating behavioral rhythms in Drosophila. *Neuron* 29(2):453–467.
8. Maywood ES, et al. (2011) Tuning the period of the mammalian circadian clock: Additive and independent effects of CK1εTau and Fbxl3Afh mutations on mouse circadian behavior and molecular pacemaking. *J Neurosci* 31(4):1539–1544.
9. Harms E, Kivimäe S, Young MW, Saez L (2004) Posttranscriptional and posttranslational regulation of clock genes. *J Biol Rhythms* 19(5):361–373.
10. Eide EJ, et al. (2005) Control of mammalian circadian rhythm by CKIepsilon-regulated proteasome-mediated PER2 degradation. *Mol Cell Biol* 25(7):2795–2807.
11. Reischl S, et al. (2007) Beta-TrCP1-mediated degradation of PERIOD2 is essential for circadian dynamics. *J Biol Rhythms* 22(5):375–386.
12. Toh KL, et al. (2001) An hPer2 phosphorylation site mutation in familial advanced sleep phase syndrome. *Science* 291(5506):1040–1043.
13. Xu Y, et al. (2005) Functional consequences of a CKIdelta mutation causing familial advanced sleep phase syndrome. *Nature* 434(7033):640–644.
14. Lowrey PL, et al. (2000) Positional syntenic cloning and functional characterization of the mammalian circadian mutation tau. *Science* 288(5465):483–492.
15. Meng QJ, et al. (2008) Setting clock speed in mammals: the CK1 epsilon tau mutation in mice accelerates circadian pacemakers by selectively destabilizing PERIOD proteins. *Neuron* 58(1):78–88.
16. Zhou M, Kim JK, Eng GW, Forger DB, Virshup DM (2015) A Period2 Phosphoswitch Regulates and Temperature Compensates Circadian Period. *Mol Cell* 60(1):77–88.
17. Huang N, et al. (2012) Crystal structure of the heterodimeric CLOCK:BMAL1 transcriptional activator complex. *Science* 337(6091):189–194.
18. Lee C, Etchegaray JP, Cagampang FR, Loudon AS, Reppert SM (2001) Posttranslational mechanisms regulate the mammalian circadian clock. *Cell* 107(7):855–867.
19. Hennig S, et al. (2009) Structural and functional analyses of PAS domain interactions of the clock proteins Drosophila PERIOD and mouse PERIOD2. *PLoS Biol* 7(4):e94.
20. Kucera N, et al. (2012) Unwinding the differences of the mammalian PERIOD clock proteins from crystal structure to cellular function. *Proc Natl Acad Sci USA* 109(9):3311–3316.
21. Ohsaki K, et al. (2008) The role of beta-TrCP1 and beta-TrCP2 in circadian rhythm generation by mediating degradation of clock protein PER2. *J Biochem* 144(5):609–618.
22. Bacon Y, et al. (2004) Screening for novel ENU-induced rhythm, entrainment and activity mutants. *Genes Brain Behav* 3(4):196–205.
23. Maywood ES, Chesham JE, Smyllie NJ, Hastings MH (2014) The Tau mutation of casein kinase 1ε sets the period of the mammalian pacemaker via regulation of Period1 or Period2 clock proteins. *J Biol Rhythms* 29(2):110–118.
24. Bae K, et al. (2001) Differential functions of mPer1, mPer2, and mPer3 in the SCN circadian clock. *Neuron* 30(2):525–536.
25. Oster H, Yasui A, van der Horst GT, Albrecht U (2002) Disruption of mCry2 restores circadian rhythmicity in mPer2 mutant mice. *Genes Dev* 16(20):2633–2638.
26. Meng QJ, et al. (2010) Entrainment of disrupted circadian behavior through inhibition of casein kinase 1 (CK1) enzymes. *Proc Natl Acad Sci USA* 107(34):15240–15245.
27. Hura GL, et al. (2009) Robust, high-throughput solution structural analyses by small angle X-ray scattering (SAXS). *Nat Methods* 6(8):606–612.
28. Monecke S, Brewer JM, Krug S, Bittman EL (2011) Duper: A mutation that shortens hamster circadian period. *J Biol Rhythms* 26(4):283–292.
29. Chen R, et al. (2009) Rhythmic PER abundance defines a critical nodal point for negative feedback within the circadian clock mechanism. *Mol Cell* 36(3):417–430.
30. Medical Research Council (1993) *Responsibility in the Use of Animals for Medical Research* (Medical Research Council, London).
31. Yamaguchi S, et al. (2003) Synchronization of cellular clocks in the suprachiasmatic nucleus. *Science* 302(5649):1408–1412.
32. Yoo SH, et al. (2004) PERIOD2::LUCIFERASE real-time reporting of circadian dynamics reveals persistent circadian oscillations in mouse peripheral tissues. *Proc Natl Acad Sci USA* 101(15):5339–5346.
33. Godinho SI, et al. (2007) The after-hours mutant reveals a role for Fbxl3 in determining mammalian circadian period. *Science* 316(5826):897–900.
34. Hirano A, et al. (2013) FBXL21 regulates oscillation of the circadian clock through ubiquitination and stabilization of cryptochromes. *Cell* 152(5):1106–1118.
35. Nolan PM, et al. (2000) A systematic, genome-wide, phenotype-driven mutagenesis programme for gene function studies in the mouse. *Nat Genet* 25(4):440–443.
36. Schneidman-Duhovny D, Hammel M, Tainer JA, Sali A (2013) Accurate SAXS profile computation and its assessment by contrast variation experiments. *Biophys J* 105(4):962–974.
37. Petoukhov MV, et al. (2012) New developments in the ATSAS program package for small-angle scattering data analysis. *J Appl Cryst* 45(Pt 2):342–350.
38. Pettersen EF, et al. (2004) UCSF Chimera–a visualization system for exploratory research and analysis. *J Comput Chem* 25(13):1605–1612.
39. Frottin F, et al. (2006) The proteomics of N-terminal methionine cleavage. *Mol Cell Proteomics* 5(12):2336–2349.
40. Huynh K, Partch CL (2015) Analysis of protein stability and ligand interactions by thermal shift assay. *Curr Protoc Protein Sci* 79:28.9.1–28.9.14.

Supporting Information

Militi et al. 10.1073/pnas.1517549113

SI Methods

ENU Mutagenesis and Wheel-Running Activity Screen. Briefly, male BALB/c mice were injected i.p. with two weekly injections of 100 mg/kg ENU (Sigma) at ∼10 wk of age (35). After a period of temporary sterility (about 15 wk), they were crossed to C3H females, and the F1 progeny were screened for abnormal circadian behavior from 6 to 12 wk of age. To test inheritance of an abnormal phenotype, F1 founder mice were backcrossed to C3H mice and the backcross progeny were assessed for the inheritance of the abnormal phenotype. Mutant mouse lines were also transferred onto a C55BL/6J background once they could be genotyped. Screens were carried out by transferring the mice to individual cages equipped with running wheels and maintained within light-tight ventilated chambers with timer-controlled lighting. Wheel-running data were collected and analyzed using Clocklab (Actimetric Software).

Genotyping. For genotyping *Edo* mice, ear biopsy DNA was subjected to a PCR discrimination assay, with amplification of exon 9 and the flanking region of *Per2* by the primers 5′ TTGAGTATTTCCCTAGTTATTGCAG 3′ and GCGACACGGAGGACACAG, followed by *HinfI* digest. Agarose gel electrophoresis revealed bands of 241 bp (WT), 241 bp, 144 bp, and 97 bp (heterozygote) and of 144 bp and 97 bp (homozygote). Genotyping for other lines was as described (24, 26, 31, 32).

RNA Extraction, RT, and Real-Time PCR. Homozygous *Edo* mutants and littermate controls on a 12-h/12-h L/D cycle were killed at 4-h intervals by cervical dislocation, and livers were harvested, dissected, immediately snap-frozen on dry ice, and stored at −80 °C. RNA was extracted using the standard TRIzol extraction protocol (Life Technologies). The total RNA concentration was determined using a nanodrop ND-1000 (Thermo Fisher Scientific). mRNA expression was determined using SYBR Green RT-PCR assays utilizing the following primers:

Bmal1 (forward: CCGTGCTAAGGATGGCTGTT, reverse: TTGGCTTGTAGTTTGCTTCTGTGT)

Cry1 (forward: GTGGATCAGCTGGGAAGAAG, reverse: CACAGGGCAGTAGCAGTGAA)

Dbp (forward: GAGCCTTCTGCAGGGAAACA, reverse: GCCTTGCGCTCCTTTTCC)

Nr1d1 (forward: CGTTCGCATCAATCGCAACC, reverse: GATGTGGAGTAGGTGAGGTC)

Per1 (forward: CCCCTGCCTCCCAGTGA, reverse: CTGAAAGTGCATCCTGATTGGA)

Per2 (forward: AGCTACACCACCCCTTACAAGCT, reverse: GACACGGCAGAAAAAAGATTTCTC)

Housekeeping control gene *Rlpl3a* (forward: TGCTGCTCTCAAGGTTGTTC, reverse: TGCTTCTTCTTCGATAGTGC).

The RT reactions were conducted using a SuperScript III First-Strand Synthesis for qRT-PCR kit with 1 μg of RNA (protocol for part 11752-050; Life Technologies). The RT-PCR reactions were performed in triplicate using 10 μL of 2× Power SYBR Green PCR Master Mix (Life Technologies), 2 μL of product from the RT reaction (diluted 1:4), 1 μL of 2 μM primer mix (containing both the forward and reverse primers), and 7 μL of nuclease-free water. A sample minus RT buffer was used as a negative control for the RT-PCR reactions. None of the negative controls reached threshold by 45 cycles. RT-PCR reactions were run on a 7500 Fast Real-Time PCR System (Applied Biosystems) in 96-well format. Relative expression was calculated using the standard $2^{-(\Delta(Ct))}$ cycle threshold relative expression method in Microsoft Excel. The relative expression of the individual samples was normalized to the *Rlpl3a*.

Plasmids. Plasmids for *Per2*-HA, *Bmal1*-Flag, and CK1ε were a gift from Filippo Tamanini (Erasmus University Medical Center, Rotterdam, The Netherlands). V5-YFP-His epitope–tagged *mPer2* and *mCry2*-HA were generated in-house. To create the mREV-ERBA-V5-His expression vector, *Rev-erba* cDNA was PCR-amplified using primer pairs 5′-CAACATGACGACCCTGGACTCC-3′ and 5′-CTGGGCGTCCACCGGGAA-3′ and cloned into a pENTR/D-TOPO vector using a pENTR Directional TOPO Cloning Kit (K2400; Invitrogen) to produce an entry clone. The latter, containing an *Rev-erba* gene, was then introduced into the pcDNA-DEST40 expression vector by following the Gateway Technology with Clonase II (12535-029; Invitrogen). Similarly, the bTRCP1-V5-His expression vector was created by amplifying *βTrcp1* cDNA from primer pairs 5′-CACCATGGACCCGGCAGAGGCGGTG-3′ and 5′-TCTGGAGATGTAGGTGTATGT-3′ and subcloned as above. The sequences of pENTR/D-TOPO and pcDNA-DEST40 vectors are available for downloading from the Invitrogen web site (www.thermofisher.com).

Site-Directed Mutagenesis. Amino acid substitution in the mPER2 PAS-B domain of mPER2 (full)-V5-YFP-His and HA-mPER2 (full) was generated using a QuikChange XL Site-Directed Mutagenesis Kit (Stratagene) according to the manufacturer's directions. Mutagenesis primers for the Edo mutant were 5′-CTCAGGAGGGTTTCTAGGCGCTTCATAGCC-3′ and its complementary strand. The presence of the expected base pair substitution was confirmed by DNA sequencing.

Size-Exclusion Chromatography. For estimation of dimerization state by size-exclusion chromatography, purified proteins were injected on a Superdex 75 10/300 GL analytical column at 160 μM (∼6.4 mg/mL) in 25 mM Hepes (pH 7.5), 200 mM NaCl, and 5 mM DTT. All size-exclusion columns were calibrated with a low-molecular-weight gel filtration standards kit (GE Healthcare Life Sciences).

SAXS. SAXS data were collected on the SIBYLS beamline (12.3.1) at the Advanced Light Source (Lawrence Berkeley National Laboratory). Multiple exposures of three concentrations (1, 3, and 5 mg/mL) of freshly purified protein were taken to check for concentration dependence of scattering and radiation damage (neither was detected). After buffer subtraction, experimental scattering curves were compared with a theoretical scattering curve derived from the X-ray crystal structure (Protein Data Bank ID code 3GDI) using FoXS (36), giving a χ fit of 16.0. To improve on the fit, AllosMod FoXS was used to build in the missing loops from the crystal structure, improving the χ fit to 2.70. Scattering data were further analyzed using the ATSAS suite of programs (37). Briefly, data were merged using PRIMUS, and the radius of gyration was determined using the Guinier approximation. The pair-distance distribution function [P(r)] and maximal particle size (D_{max}) were generated in GNOM, and the output data were used by GASBOR to calculate 10 independent solution envelopes that were averaged together using DAMAVER. The improved model of the solution structure was used in UCSF Chimera (38) to fit into the averaged solution envelope. Scattering datasets, analysis, and models have been deposited with BioISIS (www.bioisis.net)

with the following deposition codes: PLCSWP ($PER2^{WT}$) and PLCSEP ($PER2^{Edo}$).

Limited Proteolysis. Limited proteolysis of purified proteins was performed at 1.5 mg/mL in 25 mM Hepes (pH 7.5), 200 mM NaCl, and 5 mM DTT with sequencing-grade proteases (Promega) for 1 h at room temperature with the following mass (wt/wt) ratios: chymotrypsin (1:25, 1:50, and 1:100) or trypsin (1:100, 1:250, and 1:500). To visualize proteins by Coomassie staining, reactions were quenched with addition of an equal volume of 2× SDS Laemmli buffer (Bio-Rad) and samples were boiled at 95 °C for 5 min. Digested fragments were resolved by 18% SDS/PAGE and visualized by Coomassie staining. For immunoblotting, the same gel samples were first diluted 50-fold in 1× SDS Laemmli buffer and then separated by 18% SDS/PAGE and transferred to a nitrocellulose membrane. Immunoblotting was performed using anti-His_6 1:2,000 (AM1010a; Abgent). Secondary Ab was HRP-conjugated anti-mouse (A9917; Sigma) at a 1:10,000 dilution, spiked with a 1:10,000 dilution of anti-Streptactin-HRP (161-0380; Bio-Rad) for direct visualization of Western C protein markers (Bio-Rad). Chemiluminescence was detected with Clarity reagent (Bio-Rad) and detected via a CCD camera on a ChemiDoc gel imaging system (Bio-Rad).

Proteolytic samples for MS were quenched by addition of formic acid to a final concentration of 1% (vol/vol). Samples were desalted and separated by HPLC (Surveyor; Thermo Finnegan) on a Proto 300 C4 reverse-phase column with a 100-mm × 2.1-mm inner diameter and 5-μm particle size (Higgins Analytical, Inc.) using a mobile phase consisting of solvent A (0.1% formic acid in HPLC grade water) and solvent B (0.1% formic acid in acetonitrile). The samples were analyzed on an LTQ Orbitrap linear ion trap mass spectrometer system (Thermo Finnegan). Proteins were detected by full-scan MS mode (over an m/z of 300–2,000) in positive mode with the electrospray voltage set to 5 kV. Mass measurements of deconvoluted electrospray ionization mass spectra of the reversed-phase peaks were generated by Magtran software. Observed masses were within 0.01% error of calculated masses after accounting for cleavage of the N-terminal methionine (loss of 131 Da), a common occurrence for proteins expressed recombinantly in *E. coli* (39).

Differential Scanning Fluorimetry. Stability of purified proteins was assessed by miniaturized differential scanning fluorimetry using SYPRO Orange dye (Sigma–Aldrich) (40). Proteins were diluted to 10 μM with 25 mM Hepes (pH 7.5), 200 mM NaCl, 5 mM DTT, and SYPRO Orange dye at a final concentration of twofold. Fifty-microliter aliquots of $PER2^{WT}$ and $PER2^{Edo}$ were plated in replicate ($n = 6$) into a 96-well PCR plate and sealed with optically clear film (Invitrogen). Thermal denaturation was performed in a ViiA7 Real-Time PCR instrument (Applied Biosystems) using changes to the default Melt Curve program as previously described (40). Raw fluorescence data were processed in Microsoft Excel, and T_ms were obtained by nonlinear regression of sigmoidal denaturation curves using GraphPad Prism 6 as previously described (40). Data shown are representative of three independent assays. The equilibrium constant for unfolding (K_U) was determined after estimating the fraction of protein unfolded (F_U) as a function of temperature using the following equation:

$$F_U = (Fl_{obs} - Fl_{native}) / (Fl_{unfolded} - Fl_{native}),$$

where Fl_{obs} corresponds to the fluorescence observed at a given temperature, Fl_{native} is the baseline fluorescence for natively folded protein, and $Fl_{unfolded}$ corresponds to fluorescence at the upper plateau (determined after subtraction of postpeak fluorescence quenching). K_U was determined with the following equation:

$$K_U = F_U / (1 - F_U),$$

and used to calculate the free energy for unfolding of WT and *Edo* protein at the T_m for WT PER2 PAS-AB domain (~55 °C).

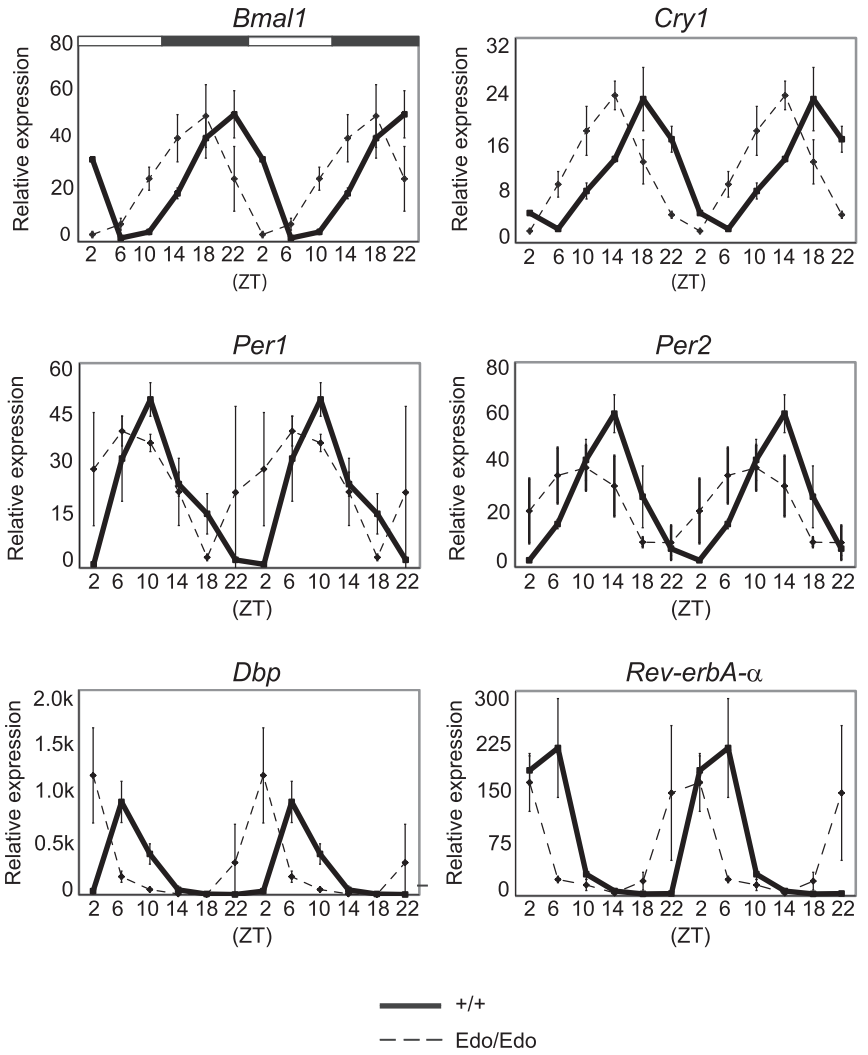

Fig. S1. Circadian gene expression in the liver of *Per2*$^{+/+}$ and *Per2*$^{Edo/Edo}$ mice. Relative expression of core oscillator and clock-controlled genes in *Per2*$^{+/+}$ (solid lines) or *Per2*$^{Edo/Edo}$ (dashed lines) in ex vivo liver samples collected at six time points across the 12-h L/D cycle. Each value represents the mean ± SEM (n = 3 independent samples). Graphs are double-plotted for clarity. ZT, Zeitgeber time.

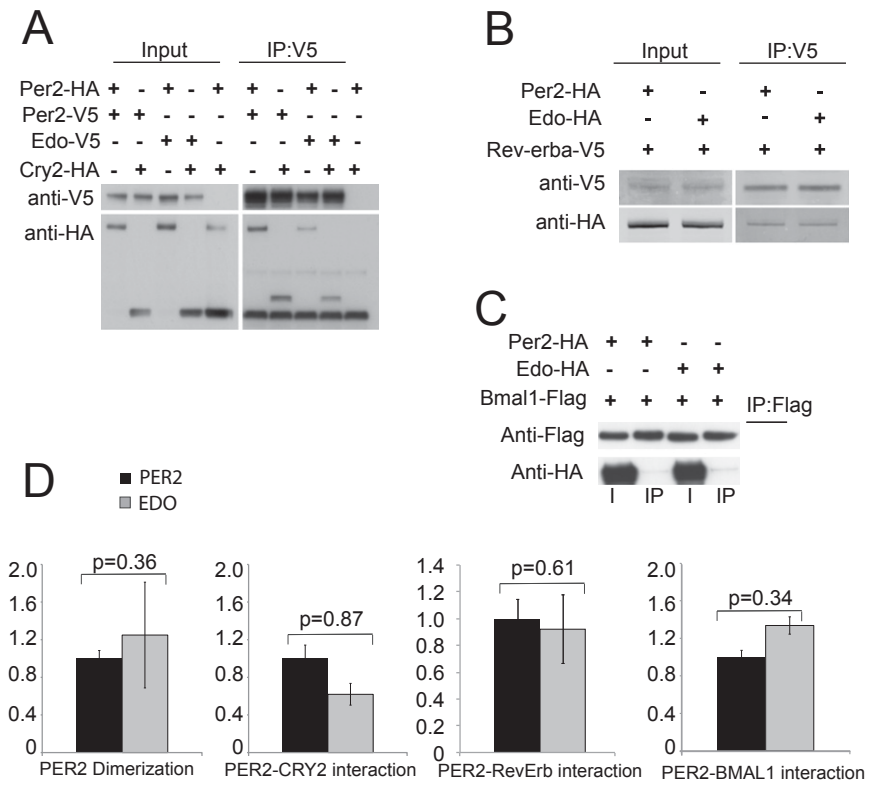

Fig. S2. PER2^{Edo} maintains an ability to dimerize and form complexes with other clock proteins. (*A*) Representative Western blots of lysates (Input) from COS7 cells transfected with either WT (Per2) or mutant (Edo) PER2-V5 and either PER2-HA or CRY2-HA immunoprecipitated (IP) with an Ab to V5. Lane 5 is a negative control. (*B*) Representative Western blots of lysates from COS7 cells transfected with either WT (Per2) or mutant (Edo) PER2-HA and REV-ERBα-V5 immunoprecipitated with an Ab to V5. (*C*) Representative Western blots of lysates from COS7 cells transfected with either WT (Per2) or mutant (Edo) PER2-HA and Flag-tagged BMAL1 immunoprecipitated with an Ab to FLAG. I, input. (*D*) Relative differences in protein interactions were determined by normalizing the amount of coimmunoprecipitated proteins to the amount of the primary precipitated protein. Values represent the mean ± SEM of four independent experiments. No significant differences were identified between Per2^{WT} and Per2^{Edo} (*t* test, *P* values as shown).

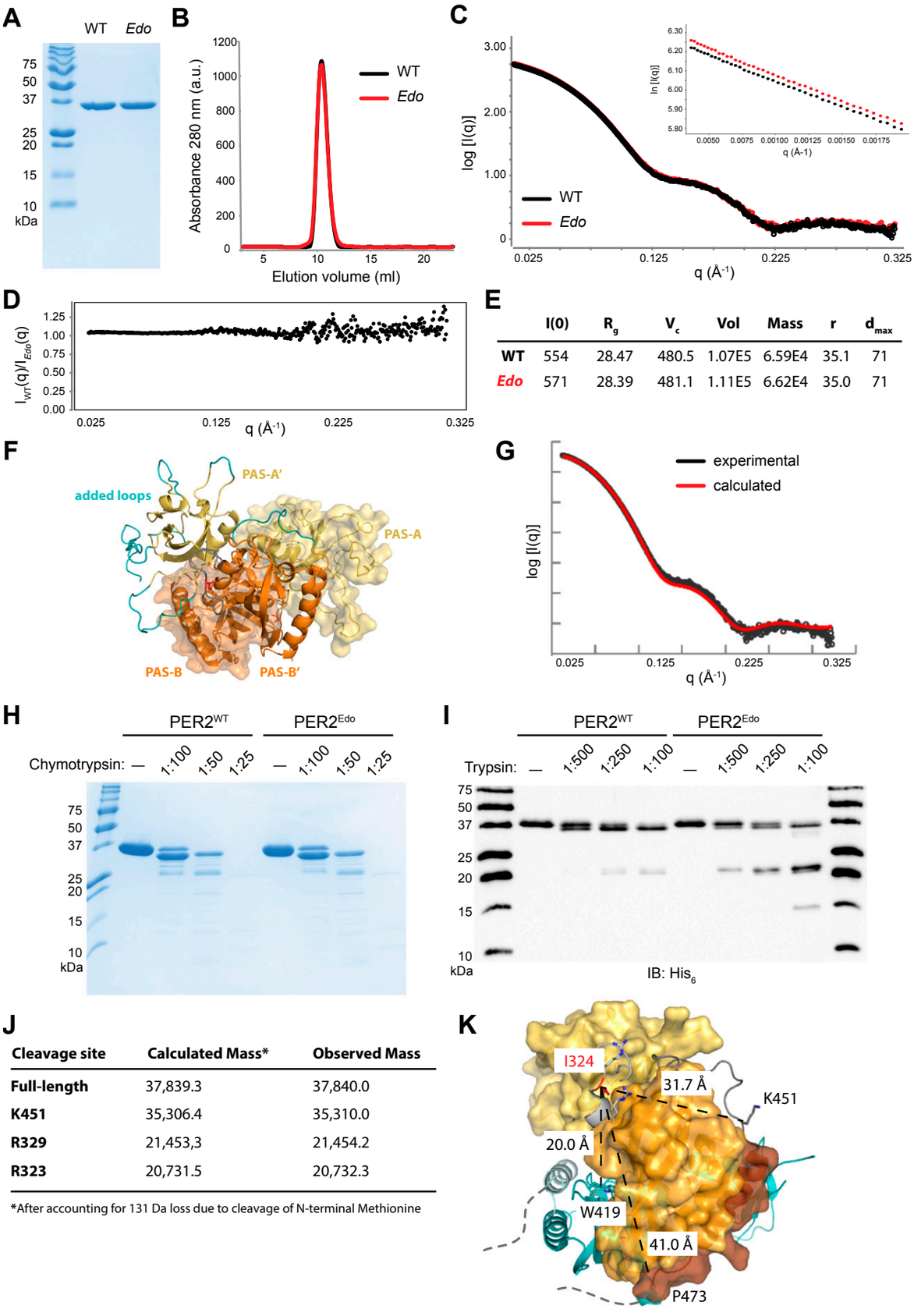

Cleavage site	Calculated Mass*	Observed Mass
Full-length	37,839.3	37,840.0
K451	35,306.4	35,310.0
R329	21,453,3	21,454.2
R323	20,731.5	20,732.3

*After accounting for 131 Da loss due to cleavage of N-terminal Methionine

Fig. S3. PAS-AB domains of PER2^{Edo} maintain a similar overall structure as the WT protein. (*A*) Recombinant PER2^{WT} and PER2^{Edo} PAS-AB domains visualized by Coomassie staining after separation by 18% SDS/PAGE. (*B*) PER2^{WT} and PER2^{Edo} migrate identically down a Superdex 75 10/300 GL analytical column. a.u., arbitrary units. (*C*) Merged scattering curves from multiple SAXS exposures taken from 1–5 mg/mL PER2^{WT} (black) and PER2^{Edo} (red). (*Inset*) Guinier plot of scattering data is linear, indicating the absence of radiation damage. (*D*) Comparison of SAXS scattering over all q values. A value of 1 for the comparison represents identical data. I_{Edo}, scattering intensity (I) for Edo mutant; I_{WT}, scattering intensity (I) for WT protein. (*E*) Table of parameters derived from analysis of SAXS data. D_{max}, maximal particle size (in angstroms); I(0), extrapolated scattering intensity at zero scattering angle q; r, particle radius (in angstroms); R_g, radius of gyration; V_c, volume of correlation; Vol, volume. (*F*) Loops missing from the PER2 crystal structure (Protein Data Bank ID code 3GDI) were modeled using AllosMod FoXS (36) to find the top 10 models that best fit the SAXS data. The model shown here represents the best fit to the SAXS data ($\chi = 2.70$). One monomer is shown in surface representation and the other as a cartoon with PAS-A domains (yellow), PAS-B domains (orange), and interdomain linker (gray) with I324 in red. Added loops are depicted on one monomer in teal. (*G*) Comparison of experimental scattering curve with the curve calculated from the structure shown in *F*. (*H*) Limited proteolysis of PER2^{WT} and PER2^{Edo} by chymotrypsin. TEV-cleaved (tagless) proteins were digested with the indicated concentrations of chymotrypsin (wt/wt) relative to PER2. (*I*) *Edo* causes differential trypsin proteolysis of the C-terminal Jα helix and interdomain linker. An immunoblot (IB) of the His_6 tag on purified proteins digested with trypsin (1:50 dilution of samples visualized by Coomassie staining in Fig. 3*D*) shows that both proteins retain the N-terminal His_6 tag. (*J*) Table of trypsin cleavage sites in His_6-PER2 PAS-AB domain based on liquid chromatography/MS analysis. (*K*) Proximity of *Edo* mutation site (I324N) to relevant functional sites on the PER2 PAS-AB dimer. One monomer of the dimer is shown in surface representation (same coloring as in Fig. 3*F*), and the other is shown in cyan as a cartoon representation. Distances are shown between I324 and (*i*) the dimer interface at W419 (19); (*ii*) the trypsin cleavage site at K451 in the linker to the Jα helix; and (*iii*) P473, the last residue of the structure before the CK1ε-dependent phosphodegron (16). Note that the Jα helix and phosphodegron from the cyan monomer are also located in close proximity to the W419 dimerization interface on the left.